Research Article | Vol. 8, No. 8 | 1 Aug 2018 | OPTICAL MATERIALS EXPRESS 2276
Optical Materials EXPRESS

Group IV mid-infrared photonics [Invited]

G. Z. Mashanovich,[1,2,*] M. Nedeljkovic,[1] J. Soler-Penades,[1] Z. Qu,[1] W. Cao,[1] A. Osman,[1] Y. Wu,[1] C. J. Stirling,[1] Y. Qi,[1] Y. Xu-Cheng,[3] L. Reid,[1] C. G. Littlejohns,[1,4] J. Kang,[5] Z. Zhao,[5] M. Takenaka,[5] T. Li,[6] Z. Zhou,[6] F. Y. Gardes,[1] D. J. Thomson,[1] and G. T. Reed[1]

[1]*Optoelectronics Research Centre, University of Southampton, Southampton SO17 1BJ, UK*
[2]*School of Electrical Engineering, University of Belgrade, 11120 Belgrade, Serbia*
[3]*Electronics and Computer Sciences, University of Southampton, Southampton SO17 1BJ, UK*
[4]*Silicon Technologies Centre of Excellence, Nanyang Technological University, 639798 Singapore, Singapore*
[5]*Department of Electrical Engineering and Information Systems, University of Tokyo, Tokyo 113-0033, Japan*
[6]*State Key Laboratory of Advanced Optical Communication Systems and Networks, School of Electronics Engineering and Computer Science, Peking University, Beijing 100871, China*
*g.mashanovich@soton.ac.uk

Abstract: In this paper we review our recent results on group IV mid-infrared photonic devices. In particular, passive structures suitable for long wavelength operation, such as suspended Si, Ge-on-Si and suspended Ge, are analyzed. In addition, Ge-on-insulator waveguides have been characterized at 3.8 μm. Several active devices have been also realized: optical modulators in silicon and germanium, and silicon and graphene detectors operating at shorter mid-IR wavelengths.

OCIS codes: (130.0130) Integrated optics; (040.3060) Infrared; (130.5990) Semiconductors.

References and links

1. R. Soref, "Mid-infrared photonics in silicon and germanium," Nat. Photonics **4**(8), 495–497 (2010).
2. G. Z. Mashanovich, M. M. Milošević, M. Nedeljkovic, N. Owens, B. Xiong, E.-J. Teo, and Y. Hu, "Low loss silicon waveguides for the mid-infrared," Opt. Express **19**(8), 7112–7119 (2011).
3. M. Nedeljkovic, A. Z. Khokhar, Y. Hu, X. Chen, J. Soler Penades, S. Stankovic, D. J. Thomson, F. Y. Gardes, H. M. H. Chong, G. T. Reed, and G. Z. Mashanovich, "Silicon photonic devices and platforms for the mid-infrared," Opt. Mater. Express **3**(9), 1205–1214 (2013).
4. G. Z. Mashanovich, F. Y. Gardes, D. J. Thomson, H. Youfang, L. Ke, M. Nedeljkovic, J. Soler Penades, A. Z. Khokhar, C. J. Mitchell, S. Stankovic, R. Topley, S. A. Reynolds, W. Yun, B. Troia, V. M. N. Passaro, C. G. Littlejohns, T. Dominguez Bucio, P. R. Wilson, and G. T. Reed, "Silicon photonic waveguides and devices for near- and mid-IR applications," IEEE J. Sel. Top. Quantum Electron. **21**(4), 1–12 (2015).
5. T. Baehr-Jones, A. Spott, R. Ilic, A. Spott, B. Penkov, W. Asher, and M. Hochberg, "Silicon-on-sapphire integrated waveguides for the mid-infrared," Opt. Express **18**(12), 12127–12135 (2010).
6. F. Li, S. D. Jackson, C. Grillet, E. Magi, D. Hudson, S. J. Madden, Y. Moghe, C. O'Brien, A. Read, S. G. Duvall, P. Atanackovic, B. J. Eggleton, and D. J. Moss, "Low propagation loss silicon-on-sapphire waveguides for the mid-infrared," Opt. Express **19**(16), 15212–15220 (2011).
7. R. Shankar, I. Bulu, and M. Lončar, "Integrated high-quality factor silicon-on-sapphire ring resonators for the mid-infrared," Appl. Phys. Lett. **102**(5), 051108 (2013).
8. S. Khan, J. Chiles, and S. Fathpour, "Silicon-on-nitride waveguides for mid- and near-infrared integrated photonics," Appl. Phys. Lett. **102**(12), 121104 (2013).
9. Y.-C. Chang, V. Paeder, L. Hvozdara, J.-M. Hartmann, and H. P. Herzig, "Low-loss germanium strip waveguides on silicon for the mid-infrared," Opt. Lett. **37**(14), 2883–2885 (2012).
10. G. Roelkens, U. Dave, A. Gassenq, N. Hattasan, C. Hu, B. Kuyken, F. Leo, A. Malik, M. Muneeb, E. Ryckeboer, Z. Hens, R. Baets, Y. Shimura, F. Gencarelli, B. Vincent, R. Loo, J. Van Campenhout, L. Cerutti, J.-B. Rodriguez, E. Tournié, X. Chen, M. Nedeljkovic, G. Z. Mashanovich, S. Li, N. Healy, A. C. Peacock, X. Liu, R. Osgood, and W. J. Green, "Silicon-based heterogeneous photonic integrated circuits for the mid-infrared," Opt. Mater. Express **3**(9), 1523–1536 (2013).
11. M. Nedeljkovic, J. S. Penades, C. J. Mitchell, A. Z. Khokhar, S. Stankovic, T. D. Bucio, C. G. Littlejohns, F. Y. Gardes, and G. Z. Mashanovich, "Surface-grating-coupled low-loss Ge-on-Si rib waveguides and multimode interferometers," IEEE Photonics Technol. Lett. **27**(10), 1040–1043 (2015).

#323442 https://doi.org/10.1364/OME.8.002276
Journal © 2018 Received 16 Feb 2018; revised 1 Apr 2018; accepted 11 Apr 2018; published 19 Jul 2018

Optical Materials EXPRESS

12. M. Brun, P. Labeye, G. Grand, J. M. Hartmann, F. Boulila, M. Carras, and S. Nicoletti, "Low loss SiGe graded index waveguides for mid-IR applications," Opt. Express **22**(1), 508–518 (2014).
13. J. M. Ramirez, Q. Liu, V. Vakarin, J. Frigerio, A. Ballabio, X. Le Roux, D. Bouville, L. Vivien, G. Isella, and D. Marris-Morini, "Graded SiGe waveguides with broadband low-loss propagation in the mid infrared," Opt. Express **26**(2), 870–877 (2018).
14. W. Li, P. Anantha, S. Bao, K. H. Lee, X. Guo, T. Hu, L. Zhang, H. Wang, R. Soref, and C. S. Tan, "Germanium-on-silicon nitride waveguides for mid-infrared integrated photonics," Appl. Phys. Lett. **109**(24), 241101 (2016).
15. A. Spott, J. Peters, M. L. Davenport, E. J. Stanton, C. D. Merritt, W. W. Bewley, I. Vurgaftman, C. S. Kim, J. R. Meyer, J. Kirch, L. J. Mawst, D. Botez, and J. E. Bowers, "Quantum cascade laser on silicon," Optica **3**(5), 545 (2016).
16. M. Muneeb, A. Vasiliev, A. Ruocco, A. Malik, H. Chen, M. Nedeljkovic, J. S. Penades, L. Cerutti, J. B. Rodriguez, G. Z. Mashanovich, M. K. Smit, E. Tourni, and G. Roelkens, "III-V-on-silicon integrated micro - spectrometer for the 3 μm wavelength range," Opt. Express **24**(9), 9465–9472 (2016).
17. Y.-C. Chang, P. Wägli, V. Paeder, A. Homsy, L. Hvozdara, P. van der Wal, J. Di Francesco, N. F. de Rooij, and H. Peter Herzig, "Cocaine detection by a mid-infrared waveguide integrated with a microfluidic chip," Lab Chip **12**(17), 3020–3023 (2012).
18. P. Tai Lin, H.-Y. Greg Lin, Z. Han, T. Jin, R. Millender, L. C. Kimerling, and A. Agarwal, "Label-free glucose sensing using chip-scale mid-infrared integrated photonics," Adv. Mater. **4**, 1755–1775 (2016).
19. Y. Hu, T. Li, D. J. Thomson, X. Chen, J. Soler Penades, A. Z. Khokhar, C. J. Mitchell, G. T. Reed, and G. Z. Mashanovich, "Wavelength division (de)multiplexing in mid-infrared wavelength range using interleaved angled multimode interferometer on the silicon-on-insulator platform," Opt. Lett. **39**, 1406–1409 (2014).
20. J. Soler Penades, A. Z. Khokhar, M. Nedeljkovic, and G. Z. Mashanovich, "Low loss mid-infrared SOI slot waveguides," IEEE Photonics Technol. Lett. **27**, 1197–1199 (2015).
21. M. Nedeljkovic, A. V. Velasco, A. Z. Khokhar, A. Delâge, P. Cheben, and G. Z. Mashanovich, "Mid-infrared silicon-on-insulator Fourier-transform spectrometer chip," IEEE Photonics Technol. Lett. **28**(4), 528–531 (2016).
22. A. G. Griffith, R. K. W. Lau, J. Cardenas, Y. Okawachi, A. Mohanty, R. Fain, Y. H. D. Lee, M. Yu, C. T. Phare, C. B. Poitras, A. L. Gaeta, and M. Lipson, "Silicon-chip mid-infrared frequency comb generation," Nat. Commun. **6**(1), 6299 (2015).
23. M. Muneeb, X. Chen, P. Verheyen, G. Lepage, S. Pathak, E. Ryckeboer, A. Malik, B. Kuyken, M. Nedeljkovic, J. Van Campenhout, G. Z. Mashanovich, and G. Roelkens, "Demonstration of Silicon-on-insulator mid-infrared spectrometers operating at 3.8 μm," Opt. Express **21**(10), 11659–11669 (2013).
24. S. A. Miller, M. Yu, X. Ji, A. G. Griffith, J. Cardenas, A. L. Gaeta, and M. Lipson, "Low-loss silicon platform for broadband mid-infrared photonics," Optica **4**(7), 707–712 (2017).
25. Z. Cheng, X. Chen, C. Y. Wong, K. Xu, C. K. Fung, Y. M. Chen, and H. K. Tsang, "Focusing subwavelength grating coupler for mid-infrared suspended membrane waveguide," Opt. Lett. **37**(7), 1217–1219 (2012).
26. J. Soler Penadés, C. Alonso-Ramos, A. Z. Khokhar, M. Nedeljkovic, L. A. Boodhoo, A. Ortega-Moñux, I. Molina-Fernández, P. Cheben, and G. Z. Mashanovich, "Suspended SOI waveguide with sub-wavelength grating cladding for mid-infrared," Opt. Lett. **39**(19), 5661–5664 (2014).
27. J. Chiles, S. Khan, J. Ma, and S. Fathpour, "High-contrast, all-silicon waveguiding platform for ultra-broadband mid-infrared photonics," Appl. Phys. Lett. **103**(15), 151106 (2013).
28. J. S. Penades, A. Ortega-Moñux, M. Nedeljkovic, J. G. Wangüemert-Pérez, R. Halir, A. Z. Khokhar, C. Alonso-Ramos, Z. Qu, I. Molina-Fernández, P. Cheben, and G. Z. Mashanovich, "Suspended silicon mid-infrared waveguide devices with subwavelength grating metamaterial cladding," Opt. Express **24**(20), 22908–22916 (2016).
29. J. S. Penadés, A. Sánchez-Postigo, M. Nedeljkovic, A. Ortega-Moñux, J. G. Wangüemert-Pérez, Y. Xu, R. Halir, Z. Qu, A. Z. Khokhar, A. Osman, W. Cao, C. G. Littlejohns, P. Cheben, I. Molina-Fernández, and G. Z. Mashanovich, "Suspended silicon waveguides for long-wave infrared wavelengths," Opt. Lett. **43**(4), 795–798 (2018).
30. A. Gutierrez-Arroyo, E. Baudet, L. Bodiou, J. Lemaitre, I. Hardy, F. Faijan, B. Bureau, V. Nazabal, and J. Charrier, "Optical characterization at 7.7 μm of an integrated platform based on chalcogenide waveguides for sensing applications in the mid-infrared," Opt. Express **24**(20), 23109–23117 (2016).
31. A. Malik, S. Dwivedi, L. Van Landschoot, M. Muneeb, Y. Shimura, G. Lepage, J. Van Campenhout, W. Vanherle, T. Van Opstal, R. Loo, and G. Roelkens, "Ge-on-Si and Ge-on-SOI thermo-optic phase shifters for the mid-infrared," Opt. Express **22**(23), 28479–28488 (2014).
32. B. Troia, J. S. Penades, A. Z. Khokhar, M. Nedeljkovic, C. Alonso-Ramos, V. M. N. Passaro, and G. Z. Mashanovich, "Germanium-on-silicon Vernier-effect photonic microcavities for the mid-infrared," Opt. Lett. **41**(3), 610–613 (2016).
33. C. Alonso-Ramos, M. Nedeljkovic, D. Benedikovic, J. S. Penadés, C. G. Littlejohns, A. Z. Khokhar, D. Pérez-Galacho, L. Vivien, P. Cheben, and G. Z. Mashanovich, "Germanium-on-silicon mid-infrared grating couplers with low-reflectivity inverse taper excitation," Opt. Lett. **41**(18), 4324–4327 (2016).
34. L. Shen, N. Healy, C. J. Mitchell, J. S. Penades, M. Nedeljkovic, G. Z. Mashanovich, and A. C. Peacock, "Mid-infrared all-optical modulation in low-loss germanium-on-silicon waveguides," Opt. Lett. **40**(2), 268–271 (2015).

Optical Materials EXPRESS

35. L. Shen, N. Healy, C. J. Mitchell, J. S. Penades, M. Nedeljkovic, G. Z. Mashanovich, and A. C. Peacock, "Two-photon absorption and all-optical modulation in germanium-on-silicon waveguides for the mid-infrared," Opt. Lett. **40**(10), 2213–2216 (2015).
36. S. Radosavljevic, N. Teigell Beneitez, A. Katumba, M. Muneeb, M. Vanslembrouck, B. Kuyken, and G. Roelkens, "Mid-infrared Vernier racetrack resonator tunable filter implemented on a germanium on SOI waveguide platform," Opt. Mater. Express **8**(4), 824–835 (2018).
37. G. Z. Mashanovich, C. J. Mitchell, A. Z. Khokhar, C. G. Littlejohns, J. Soler Penades, W. Cao, Z. Qu, L. Shen, N. Healy, A. C. Peacock, F. Y. Gardes, V. Mittal, G. Senthil Murugan, J. S. Wilkinson, and M. Nedeljkovic, "Germanium mid-infrared photonic devices," J. Lightwave Technol. **35**(4), 624–630 (2017).
38. M. Nedeljkovic, J. S. Penades, V. Mittal, G. S. Murugan, A. Z. Khokhar, C. Littlejohns, L. G. Carpenter, C. B. E. Gawith, J. S. Wilkinson, and G. Z. Mashanovich, "Germanium-on-silicon waveguides operating at mid-infrared wavelengths up to 8.5 μm," Opt. Express **25**(22), 27431–27441 (2017).
39. J. Kang, M. Takenaka, and S. Takagi, "Novel Ge waveguide platform on Ge-on-insulator wafer for mid-infrared photonic integrated circuits," Opt. Express **24**(11), 11855–11864 (2016).
40. S. Kim, J.-H. Han, J.-P. Shim, H.-J. Kim, and W. J. Choi, "Verification of Ge-on-insulator structure for a mid-infrared photonics platform," Opt. Mater. Express **8**(2), 440–451 (2018).
41. M. Nedeljkovic, S. Stanković, C. Mitchell, A. Z. Khokhar, S. Reynolds, D. J. Thomson, F. Y. Gardes, C. Littlejohns, G. T. Reed, and G. Z. Mashanovich, "Mid-infrared thermo-optic modulators in SOI," IEEE Photonics Technol. Lett. **26**(13), 1352–1355 (2014).
42. J. Chiles and S. Fathpour, "Mid-infrared integrated waveguide modulators based on silicon-on-lithium-niobate photonics," Optica **1**(5), 350–355 (2014).
43. R. Soref, "Enabling 2 μm communications," Nat. Photonics **9**(6), 358–359 (2015).
44. M. A. Van Camp, S. Assefa, D. M. Gill, T. Barwicz, S. M. Shank, P. M. Rice, T. Topuria, and W. M. J. Green, "Demonstration of electrooptic modulation at 2165nm using a silicon Mach-Zehnder interferometer," Opt. Express **20**(27), 28009–28016 (2012).
45. D. J. Thomson, L. Shen, J. J. Ackert, E. Huante-Ceron, A. P. Knights, M. Nedeljkovic, A. C. Peacock, and G. Z. Mashanovich, "Optical detection and modulation at 2μm-2.5μm in silicon," Opt. Express **22**(9), 10825–10830 (2014).
46. M. Nedeljkovic, R. Soref, and G. Z. Mashanovich, "Free-carrier electrorefraction and electroabsorption modulation predictions for silicon over the 1-14-um infrared wavelength range," IEEE Photonics J. **3**(6), 1171–1180 (2011).
47. M. Nedeljkovic, R. Soref, and G. Z. Mashanovich, "Predictions of free-carrier electroabsorption and electrorefraction in germanium," IEEE Photonics J. **7**(3), 1–14 (2015).
48. R. Wang, M. Muneeb, S. Sprengel, G. Boehm, A. Malik, R. Baets, M.-C. Amann, and G. Roelkens, "III-V-on-silicon 2-μm-wavelength-range wavelength demultiplexers with heterogeneously integrated InP-based type-II photodetectors," Opt. Express **24**(8), 8480–8490 (2016).
49. A. Gassenq, F. Gencarelli, J. Van Campenhout, Y. Shimura, R. Loo, G. Narcy, B. Vincent, and G. Roelkens, "GeSn/Ge heterostructure short-wave infrared photodetectors on silicon," Opt. Express **20**(25), 27297–27303 (2012).
50. J. D. B. Bradley, P. E. Jessop, and A. P. Knights, "Silicon waveguide-integrated optical power monitor with enhanced sensitivity at 1550nm," Appl. Phys. Lett. **86**(24), 241103 (2005).
51. A. P. Knights, J. D. B. Bradley, S. H. Gou, and P. E. Jessop, "Silicon-on-insulator waveguide photodetector with self-ion-implantation-engineered-enhanced infrared response," J. Vac. Sci. Technol. A **24**(3), 783–786 (2006).
52. J. J. Ackert, D. J. Thomson, L. Shen, A. C. Peacock, P. E. Jessop, G. T. Reed, G. Z. Mashanovich, and A. P. Knights, "High-speed detection above the telecommunication windows with monolithic silicon photodiodes," Nat. Photonics **9**, 393–396 (2015).
53. X. Wang, Z. Cheng, K. Xu, H. Ki Tsang, and J.-B. Xu, "High-responsivity graphene/silicon-heterostructure waveguide photodetectors," Nat. Photonics **7**(11), 888–891 (2013).

1. Introduction

Group IV materials, such as Si, Ge, SiN, GeSn and graphene all have attractive properties for applications in the mid-IR. Si and Ge in particular are transparent up to 8 and 15 micrometers, respectively, and offer realization of compact and potentially low cost integrated circuits for a range of applications [1]. GeSn alloys and graphene complement the two by enabling integrated mid-IR sources and detectors. A number of mid-IR devices have been reported in the last few years, based on several material platforms: silicon-on-insulator (SOI) [e.g 2–4.], silicon-on-sapphire (SOS) [e.g 5–7.], silicon-on-nitride (SON) [e.g 8], germanium-on-silicon (GOS) [e.g 9–11]), SiGe-on-Si [12,13] and Ge-on-silicon nitride [14]. Integration with III-V sources and detectors has also been successfully realized [e.g 15,16], as has demonstration of simple sensing experiments [e.g 17,18].

In this paper we report our recent results on Si and Ge based mid-IR devices. In the first section, we briefly review our recently published results on SOI, suspended Si and GOS

Optical Materials EXPRESS

devices. We then present new results on passive devices: first propagation loss measurements for suspended Ge waveguides and fabrication and characterization of Ge-on-insulator (GOI) waveguides at a wavelength of 3.8 μm. In the second section, we report new results on optical modulators in Si and Ge at various wavelengths and graphene mid-IR detectors realized on the SOI platform, and also give a brief review on recently published results on defect mediated Si detectors.

2. Passive Si and Ge mid-IR devices

Due to well-developed fabrication techniques, availability of the material and experience in developing NIR photonic devices and circuits, the most suitable group IV mid-IR (MIR) platform is SOI. A series of papers and results have been published on SOI devices and circuits operating up to a wavelength of 3.9 μm [2–4, 19–22]. Waveguide losses and performance of other passive devices (MMIs, MZIs, MUXs etc) are similar to those realized in the near-IR (NIR) [e.g 23]. However, oxide has high material loss beyond 3.6 μm and although it has been recently shown that the operation wavelength of SOI could be extended to 5-6 μm [24], alternative platforms need to be considered for longer wavelength operation.

2.1 Suspended Si

One potential solution for longer wavelength operation is to remove the bottom SiO_2 cladding and to suspend Si. By doing so, the entire transparency range of Si can be exploited. The two main approaches to achieve suspended Si devices are: 1) to create rib waveguides and then etch holes on the side through the etched slab which do not perturb the optical mode and serve as access points for HF removal of the buried oxide layer [25] or 2) to implement a subwavelength approach which involves only one dry etch step, first published by J. Soler Penades et al. [26]. It is also possible to suspend Si by a bonding technique [27].

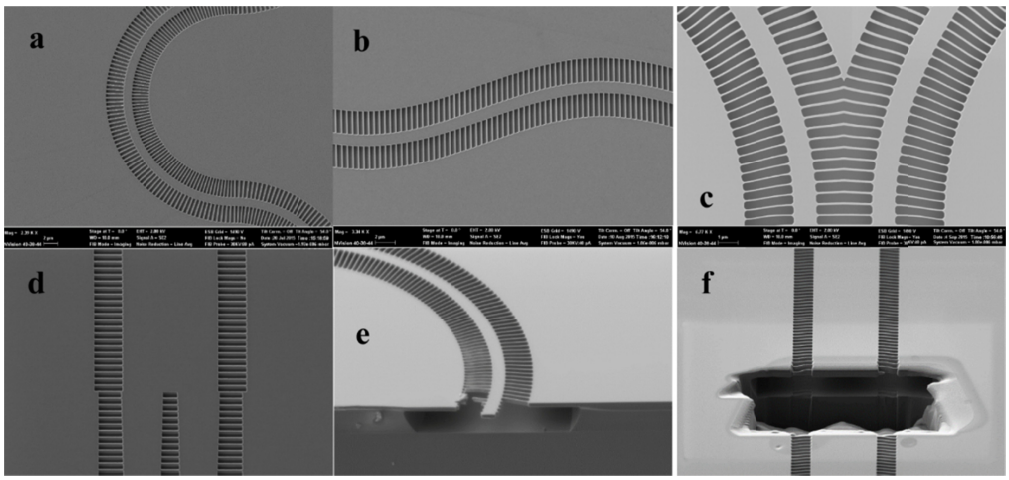

Fig. 1. SEM image of a) the 90° bend b) the s-bend c) waveguides converging towards the MMI input section and d) input section half of the MMI (top views). e) A cleaved facet of a 90° bend with the BOX locally removed, with a few destroyed silicon strips due to the cleaving. f) Under-etched multimode region of the MMI after FIB cut, with no appreciable deformation of the suspended structure [28]

The subwavelength grating (Fig. 1) has a lower effective refractive index than the core and hence provides lateral mode confinement. At the same time, the grating holes enable HF removal of the SiO_2 bottom cladding (Fig. 1(e), 1(f)). By optimizing our previous designs, in collaboration with the University of Malaga and the National Research Council of Canada, we have demonstrated several low loss passive devices at a wavelength of 3.8 μm, including waveguides, bends, grating couplers, MMIs, and MZIs, some of which are shown in Fig. 1.

Optical Materials EXPRESS

The waveguide propagation loss was 0.8 dB/cm and the 90° bend loss was only 0.01 dB/bend [28].

This demonstration was very promising and by adapting it for longer wavelengths we have recently fabricated suspended Si waveguides and bends operating at 7.7 μm using a thicker SOI platform (1.4 μm compared to 500 nm SOI from [28]). This time, the propagation loss was higher, 3.1 dB/cm [29], however we estimated that 2.1 dB/cm came from the intrinsic material absorption of Si at 7.7 μm, meaning that the loss related to scattering was ~1 dB/cm. This loss is very similar to the loss of chalcogenide [30] and GOS waveguides at the same wavelength. After this first demonstration of a low loss Si waveguide operating at such a long wavelength, our future work will involve development of other passive devices for ~8 μm and implementation of the platform for sensing as it can enable higher interaction between the evanescent optical mode and an analyte.

2.2 Ge-on-Si

The second platform suitable for longer wavelengths is GOS. Germanium can be grown on Si substrates by CVD techniques and although Si has higher material loss beyond 8 μm, based on bulk material loss data from literature, GOS waveguides should have low loss up to 11-12 μm. There have been several demonstrations of waveguides [9–11], MUXs [10] and thermo-optic modulators [31] at shorter wavelengths. SiGe waveguides operating at 7.4 μm were reported in [12], followed by a recent report on relatively thick SiGe on Si waveguides with loss of ~3 dB/cm at 8.5 μm, whilst thinner SiGe waveguides showed losses of >8 dB/cm beyond 7 μm for TE and >16 dB/cm beyond 8 μm for TM polarization [13].

Our work on this platform includes 0.6 dB/cm GOS waveguides [11], low loss MMIs [11], Vernier rings [32], and grating couplers [33] at 3.8 μm, all optical modulation [34], and TPA measurements [35] at 2-3.9 μm. S. Radosaljevic *et al.* have very recently demonstrated Vernier racetrack resonator tunable filters on a Ge-on-SOI waveguide platform operating in the 5 μm wavelength range [36]. We have recently investigated passive GOS devices at 7.5-9 μm [37,38] and found that the 3 μm GOS platform showed 2.5 dB/cm at 7.5 μm but became very lossy beyond 8 μm (>15 dB/cm) [38]. There are several potential reasons that can contribute to higher losses such as Si substrate absorption, defects/dislocations at Ge-Si interface, time dependent haze (TDH) formation, free carrier absorption or stress effects. However, our estimates did not predict that any of these should contribute significantly to the loss. Therefore, further investigation is required to find the reasons for high GOS losses beyond 8 μm.

2.3 Suspended Ge waveguides

Together with further investigation of the GOS platform and its suitability for long wavelength operation, we have recently initiated work on suspended Ge. This platform should enable operation up to 15 μm and can benefit from well-developed techniques already demonstrated in the suspended Si platform (section 2.1).

The waveguides were fabricated using 6” Ge-on-SOI wafers with a 400 nm Ge layer grown by RPCVD on 220 nm SOI. Rib waveguides were designed for single mode propagation at λ = 3.8 μm. The dimensions were: height (H) = 400 nm, width (W) = 1.1 μm and etch depth (D) = 250 nm. The SOI substrate consisted of a 220 nm thick layer of Si on a 3 μm thick layer of SiO_2. The waveguides were patterned using e-beam lithography. They were then defined by dry etching using ICP (Fig. 2(b)). A second e-beam lithography step followed in order to define the holes, which were etched down to the BOX (Fig. 2(c)). The sample then underwent two wet etch steps. First, the sample was immersed in 1:7 HF for 10 minutes, which removed the BOX (Fig. 2(d)). Then it was immersed in a 25% aqueous solution of Tetramethylammonium Hydroxide (TMAH) at room temperature for 2 hours, which resulted in a partial removal of the Si layer (Fig. 2(e)). Out of 220 nm of the initial thickness, approximately 70 nm were left. An SEM of the fabricated waveguides is shown in Fig. 3.

Optical Materials EXPRESS

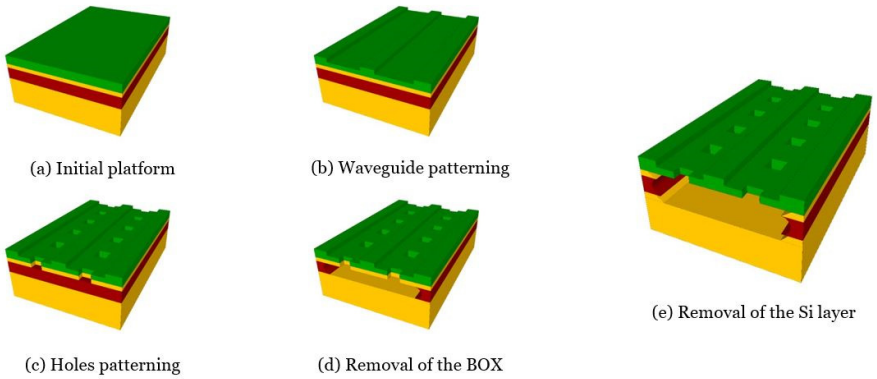

Fig. 2. Fabrication process flow for suspended Ge waveguides (green, yellow and red represent Ge, Si and BOX layers, respectively).

The waveguides were measured using the effective cut-back method. Waveguides of different lengths were fabricated for the propagation loss measurement. The measured value was 2.9 dB/cm at $\lambda = 3.8$ μm. The lab setup used for the characterisation is described in more detail in [2]. Our future work will involve improvement of the fabrication process such that Ge is grown on thinner SOI wafers resulting in a shorter TMAH etch, and development of other passive devices in this platform and its implementation for sensing at longer wavelengths.

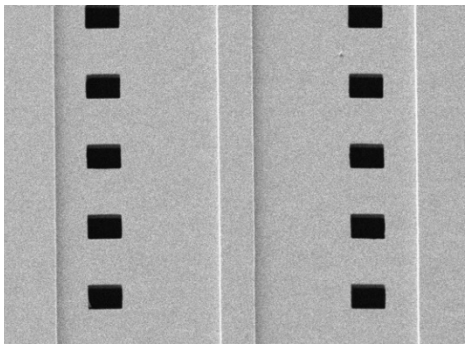

Fig. 3. SEM image of the fabricated suspended Ge waveguide.

2.4 Ge-on-insulator waveguides

The Ge-on-insulator (GOI) platform has been suggested for MIR photonics due to a large difference between the refractive indices of Ge and SiO_2 (~4.0 and ~1.4 respectively) resulting in strong confinement of light in the Ge waveguide, which is necessary to achieve compact photonic devices. Either crystalline Ge or a-Ge on SiO_2 can be used [37].

The GOI samples reported here have been fabricated as described in [39]: a SiO_2 capping layer was deposited on a bulk Ge wafer for protection; H^+ ions were implanted under the Ge surface and the SiO_2 layer removed; a 10 nm Al_2O_3 layer was deposited on the Ge surface; the Ge wafer was bonded to a Si wafer with 2 μm SiO_2 layer on the Si surface; the wafer was annealed to cause splitting along the implanted H^+ ions; the wafer underwent a chemical mechanical polishing (CMP) process to reduce the Ge surface roughness (see Fig. 4). The resulting Ge layer was 515 nm thick.

Optical Materials EXPRESS

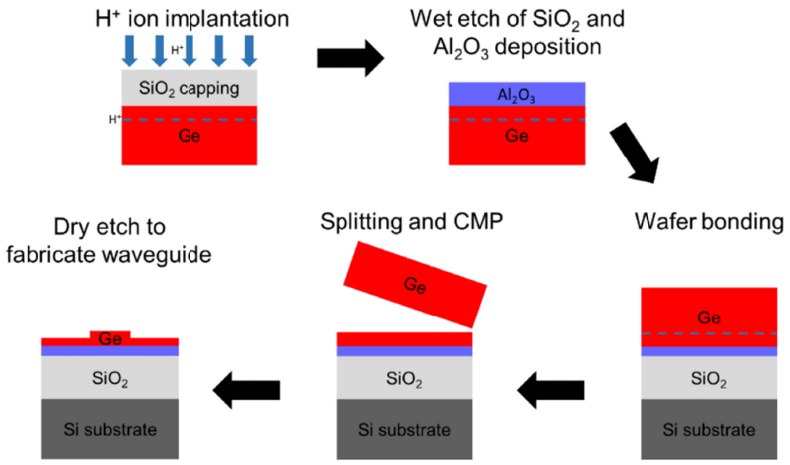

Fig. 4. Fabrication process to obtain GOI waveguides. Adapted from [39].

For single mode propagation, a rib waveguide was chosen. Simulation of the waveguide dimensions in Lumerical MODE Solutions using a waveguide height of 515 nm resulted in a 1.1 μm waveguide width and 265 nm etch depth. The propagation loss was measured by the cut-back method to be 4.5 ± 0.5 dB/cm at 3.8 μm wavelength, which is less than it was previously reported for this material platform: 14 dB/cm at 2 μm [39]. The GOI platform can be used for SWIR Ge MIR integrated circuits and for LWIR integrated circuits after suspending Ge by HF removal of the oxide bottom cladding and the intermediate Al_2O_3 layer. For longer waveguide operation it may be also possible to implement a Ge waveguide platform on Si substrates using F- and Y-based insulator claddings such as CaF_2 and Y_2O_3 [40].

3. Active group IV mid-IR devices

In this section of the paper we present new results on group IV mid-IR modulators and detectors at wavelengths of 2 μm and 3.8 μm.

3.1 Modulation in Si and Ge

To date there have been few investigations of modulation in Si or Ge in the mid-infrared [e.g 41,42]. However, there is interest in using the 2 μm wavelength range to increase the bandwidth available for fiber-based telecommunications [43]. At 2165 nm SOI carrier injection modulators operating at up to 3 Gb/s with pre-emphasis [44], and at 1950 nm GOI modulators operating under DC conditions [39] have been demonstrated.

In the near-IR, high-speed modulators typically employ free-carrier depletion in a PN junction (e.g [45]), and use either a Mach-Zehnder interferometer (MZI) or ring resonator to convert the phase change into an intensity change. We have demonstrated a MZI-based PN junction modulator in the SOI platform. The waveguides were designed to be single mode at 2 μm, and were 220 nm thick, 550 nm wide, and with a 130 nm etch depth. Inverse tapers were placed at the chip facets for fiber-to-chip coupling and y-splitters were used as 3 dB power splitters in the MZI, which allowed us to characterise the same device both at 1550 nm and at 1950 nm. The device operates at carrier depletion mode, and under a 4V DC reverse bias. We measured a modulation efficiency ($V_\pi L_\pi$) of 2.02 V.cm at 1550 nm and 2.68 V.cm at 1950 nm. The RF response was measured by applying a pseudo-random-bit-stream (PRBS) OOK signal with peak-to-peak amplitude of 4V and DC bias of –2.5 V. At 1550 nm we were able to measure an open eye diagram at 30 Gb/s, with an extinction ratio of 7.1 dB. At 1950 nm we measured an open eye diagram at 20 Gb/s with a 5.8 dB extinction ratio (shown in Fig.

Optical Materials EXPRESS

5(a)), but at that wavelength we were prevented from measuring higher speed modulation by the external InGaAs detector bandwidth.

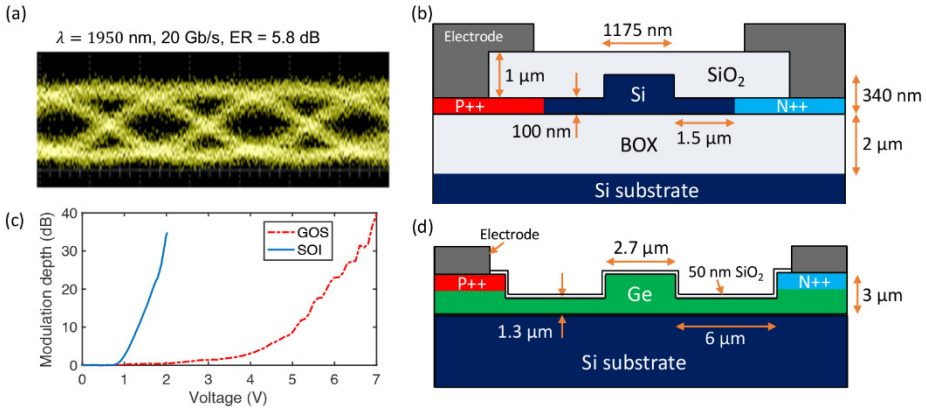

Fig. 5. (a) Experimental eye diagram showing transmission of SOI PN junction carrier depletion modulator at 1.95 µm, driven with a 20 Gb/s PRBS signal. (b) Schematic diagram of SOI PIN junction carrier injection modulator, designed for 3.8 µm wavelength. (c) Measured modulation depths of a 2 mm long SOI and a 1 mm long GOS carrier injection modulator with varying DC forward bias, both at 3.8 µm. (d) Schematic diagram of GOS PIN junction carrier injection modulator, designed for 3.8 µm wavelength.

At longer wavelengths there may be applications for modulation related to free-space communications, signal processing, and switching. Semi-empirical equations for the free-carrier effect for Si were presented in [46] and for Ge in [47], predicting that the strength of the effect would increase approximately proportionally to the square of wavelength in both materials. They also predict that the effect is generally stronger in Ge than in Si.

We have designed and fabricated modulators in SOI and GOS material platforms for 3.8 µm, in which PIN diodes are integrated with a waveguide, and carrier injection into the waveguide increases the absorption of the waveguide core. The cross-sections of the PIN diodes of the SOI and GOS devices (and their dimensions) are shown in Figs. 5(b) and 5(d), respectively. Because of the larger dimensions of the GOS waveguide it has lower lateral mode confinement, and therefore the highly doped Ohmic contact regions are placed further away to minimize the excess loss from free carrier absorption. The SOI PIN diode was 2 mm long, while the GOS diode was 1 mm long. In both devices grating couplers were used to couple light in and out of the waveguide. The transmission of each device was measured while applying varying forward bias across the PIN diode using a DC power supply. The modulation depths of both devices under varying DC forward bias are shown in Fig. 5(c), where it can be seen that both achieve a modulation depth > 30 dB. It can be seen from Fig. 5(c) that a significantly lower voltage was required to produce the same modulation depth in the SOI device, which can be attributed to a combination of the shorter diode length in the GOS modulator, the much larger waveguide dimensions and Ohmic contact separation, and potentially the shorter carrier lifetime from Ge crystal growth defects near the Ge/Si interface. The SOI PIN modulator had an insertion loss of 2.9 dB at 3779 nm, but we were unable to reliably measure the insertion loss of the GOS modulator, because the normalization waveguides on the chip were damaged during fabrication.

Optical Materials EXPRESS

3.2 Group IV mid-IR detectors

One of the most important devices in group IV MIR integrated circuits is a photodetector. Several approaches have been demonstrated so far. Following a similar approach already demonstrated in the NIR, InP detectors were bonded on SOI waveguides using BCB achieving responsivity of 1.6 A/W at 2.35 μm and dark current of 5 nA at −0.5 V [48]. In the 3-4 μm wavelength range InAsSb PIN photodiodes have been realized, again in SOI, with a responsivity of 0.3 A/W at room temperature [16]. GeSn photodetectors are group IV alternatives that offer considerable potential to extend the sensitivity of germanium technologies into the MIR. Such photodetectors have achieved responsivities of 0.1 A/W for surface illumination [49].

Silicon is traditionally limited in terms of spectral coverage (<1 μm) by its bandgap energy. However, it has been shown that Si detection can be extended towards the NIR by using three main sub-bandgap absorption mechanisms: the internal photoemission (IPE) effect, two-photon absorption (TPA) and defect-mediated absorption. The most useful monolithic approach is via introduction of lattice defects and associated deep level charge states in the silicon bandgap, which provide sub-bandgap photon absorption, and these defects can be introduced by ion implantation [e.g 50,51]. These photodiodes (PDs) are usually created in a standard SOI rib waveguide by implanting doped p + and n + regions on either side of a waveguide to form a lateral PIN diode, and then introducing defects in the waveguide core by implantation. These two regions should be placed such that they enable fast operation whilst introducing negligible excess loss due to free-carrier absorption. This defect-mediated absorption does not require heterogeneous integration, making it a robust and low-cost technology. It also allows for operation at room temperature. In collaboration with McMaster University, we have achieved significantly large bandwidth (>15 GHz) and good responsivity of 0.3 A/W at 2 μm for a photodetector based on the 220nm SOI platform and implanted with boron [52]. However, the responsivity was obtained in avalanche mode and was rather modest compared to what we have measured at 1550 nm (3 A/W), and dropped by an order of magnitude at 2.5 μm, showing that the PD structure needs significant further optimization.

By combining graphene's superior electronic and optical properties and Si and Ge platforms, photodetection can be achieved in the MIR wavelength region. A graphene on silicon waveguide based detector operating at a wavelength of 2.75 μm has previously achieved 0.13 A/W responsivity [53]. Here we present the first graphene photodetector operating at a wavelength of 3.8 μm, based on the coplanar integration method with SOI waveguides. The graphene layer was grown by CVD and transferred to the SOI waveguide.

A schematic of the device cross-section is shown in Fig. 6. The contacts to the graphene were arranged in an asymmetric metal-graphene-metal (MGM) configuration. The core of the waveguide was 1.3 μm wide and 500 nm high with a 50 nm thick slab region. A 90 nm thick PECVD SiO_2 layer was deposited for passivation and decreasing charging effects during graphene deposition. The CVD grown graphene was then transferred on the top of the chip, and patterned by reactive ion etching (RIE). Finally, 100 nm thick Au contacts were fabricated on top of the graphene on either side of the Si waveguide with a separation of 1.5 μm and 5 μm, respectively (Fig. 6). The interaction length between the SOI waveguide and the graphene layer was 500 μm.

The device was characterized with bias voltages from −1 to 1 V. Generated photocurrent was measured by a picoammeter (Keithley 6487). The photocurrent is plotted as a function of the increased optical power that was coupled into the graphene photodetector in Fig. 7. The gradient of the linear fitting gives the photoresponsivity of the device as 2.2 mA/W at 3.8 μm under a −1 V bias voltage. The optical power incident on the photodetector was calculated by taking into account the absorption from the input fiber, the coupling loss of the input grating coupler, and the loss from access waveguides.

Optical Materials EXPRESS

The responsivity of the device can be improved by optimizing the device configuration for better overlap between the optical mode and graphene, adjusting the electrode geometry, and modifying the fabrication process to improve the graphene quality. Our future work will focus on these optimizations and on achieving higher responsivity in the MIR.

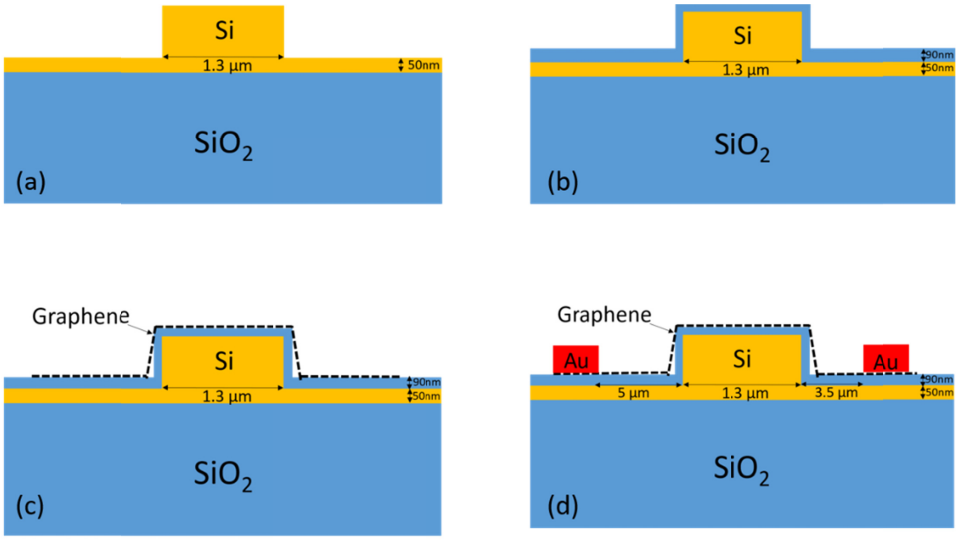

Fig. 6. Schematic cross-section of the graphene mid-IR detector.

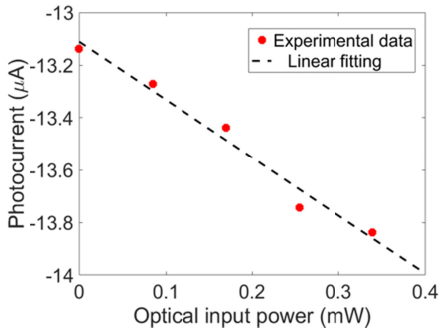

Fig. 7. Photocurrent versus optical input power coupled into the detector under −1 V bias voltage.

4. Conclusions

There are several material platforms that can be used in different parts of the MIR wavelength range. The most promising for long wavelength operation are Ge-on-Si (GOS) and suspended Ge. Higher losses have been observed in GOS for wavelengths >8 µm and further investigation is needed to determine the reasons and potential solutions for this problem. Initial results at 3.8 µm for the suspended Ge platform are promising and further work will be carried out in order to demonstrate a low loss suspended Ge platform that can be used up to 15 µm. Waveguides in Ge-on-insulator (GOI) have been fabricated and characterized at 3.8 µm. The loss of 4.5 dB/cm is the lowest measured for this platform, but is significantly higher than losses in SOI at the same wavelength (~1 dB/cm). Therefore, fabrication improvements related to wafer bonding are crucial in order to reduce the loss and make this platform an interesting solution for both shorter and longer MIR wavelengths. In terms of active group IV MIR devices, we have demonstrated the fastest optical modulators in Si to date. We have achieved 20 Gb/s with 5.8 dB extinction ratio in depletion type Si modulators at 2 µm. We

Optical Materials EXPRESS

have also fabricated injection type Si and Ge modulators at 3.8 μm and measured >30 dB extinction ratios. Defect mediated detection in Si is a promising route for the realization of monolithic MIR detectors. Graphene is another promising candidate for detection and in our first attempt we have fabricated a graphene-SOI waveguide integrated detector and measured 2.2 mA/W responsivity at 3.8 μm. Further improvements are to be investigated to increase the responsivity and to demonstrate graphene detectors at longer wavelengths.

Funding

EPSRC [MIGRATION (EP/L01162X/1); CORNERSTONE (EP/L021129/1); Electronic-Photonic Convergence (EP/N013247/1); and National Hub in High Value Photonic Manufacturing (EP/N00762X/1)]; National Research Foundation of Singapore (NRF-CRP12-2013-04); Royal Academy of Engineering (M. Nedeljkovic fellowship, RF201617/16/33).

Acknowledgements

The authors are grateful to Shaif-ul Alam and Junjia Wang from the Optoelectronics Research Centre, University of Southampton for help with building the high speed mid-IR setup.

All data supporting this study are openly available from the University of Southampton repository at https://doi.org/10.5258/SOTON/D0495.